Supplementary materials

Using near-infrared enhanced thermozyme and *scFv* dual-conjugated Au nanorods for detection and targeted photothermal treatment of Alzheimer's disease

Dongni Liu [§], Wei Li [§], Xiaoyu Jiang, Shuju Bai, Jiyang Liu, Xutong Liu, Yuhua Shi, Ziyu Kuai, Wei Kong, Renjun Gao [*] and Yaming Shan [*]

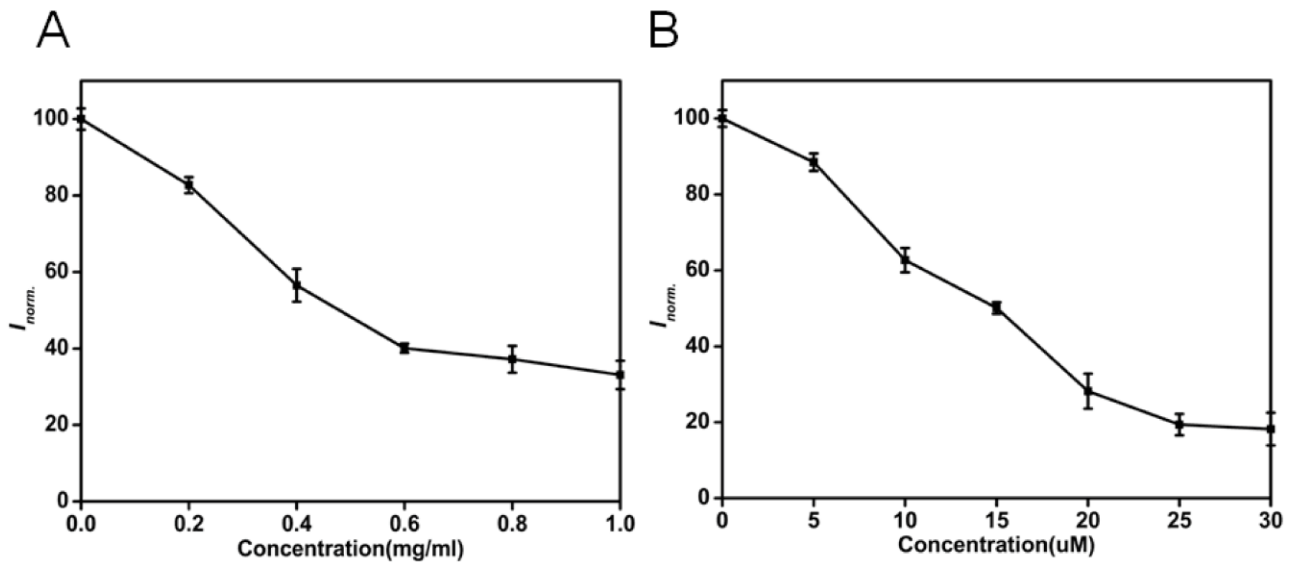

Figure S1. Different concentrations of APH and *scFv* for degradation and/or inhibition Aβ. Fibrillation kinetics of Aβ as monitored by the development of thioflavin T binding in the presence of APH (A) or *scFv* (B).

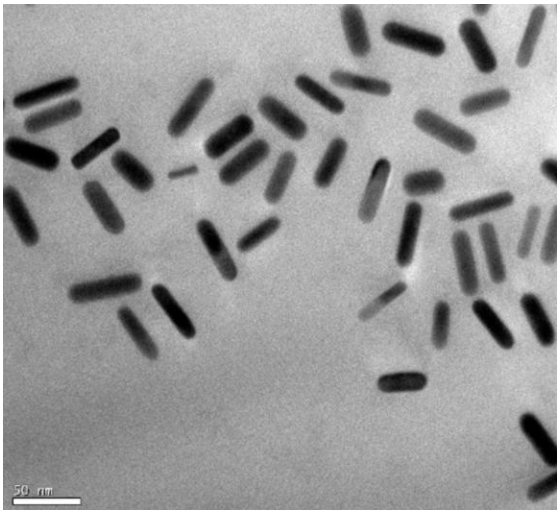

Figure S2. TEM image of as synthesized GAS.

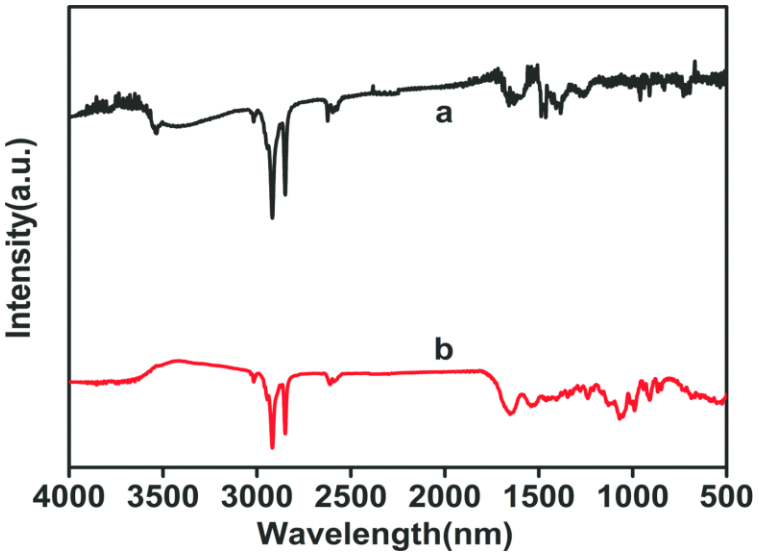

Figure S3. FTIR spectra of APH ST0779 (a) and GAS (b).

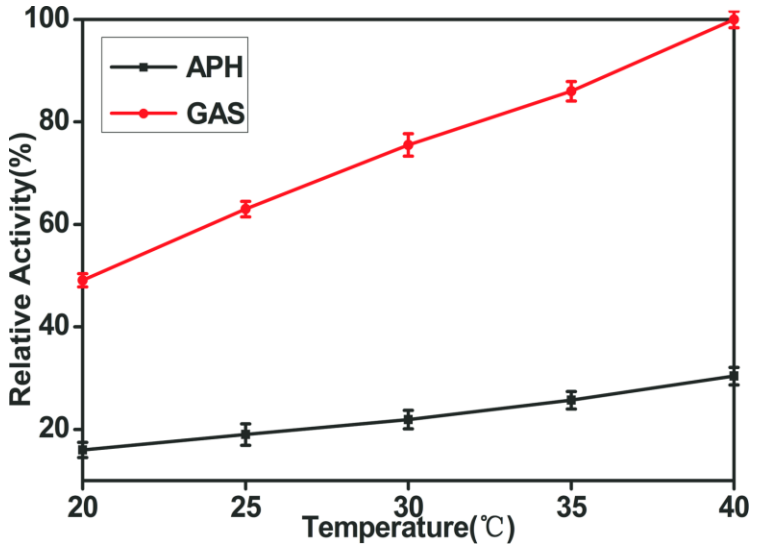

Figure S4. Relative activity of thermophilic APH heated by water bath and photothermal GAS heated by exposure to a 808nm NIR laser at the same temperature. Enzyme activity was tested with Ac-A_3 as the substrate in Tris-HCl buffer (50mmol L^{-1}, pH=8.0). Error bars indicate the standard deviation from three independent experiments.

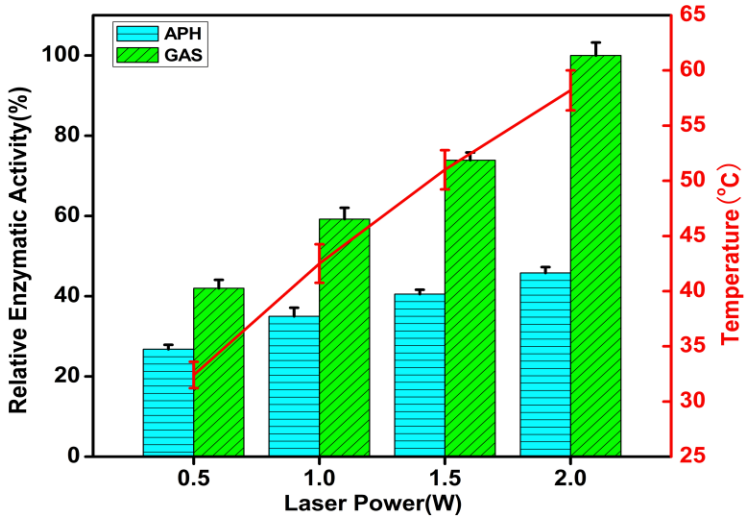

Figure S5. NIR-induced enzymatic activity of GAS aqueous solution compared with APH at different power densities. APH was heated by water bath to the same temperature as GAS heated by the photothermal effect. The concentration of GAS was 1mg/mL, in which the enzyme loading is equivalent to free APH 0.46mg/mL. Error bars indicate the standard deviation from three independent experiments.

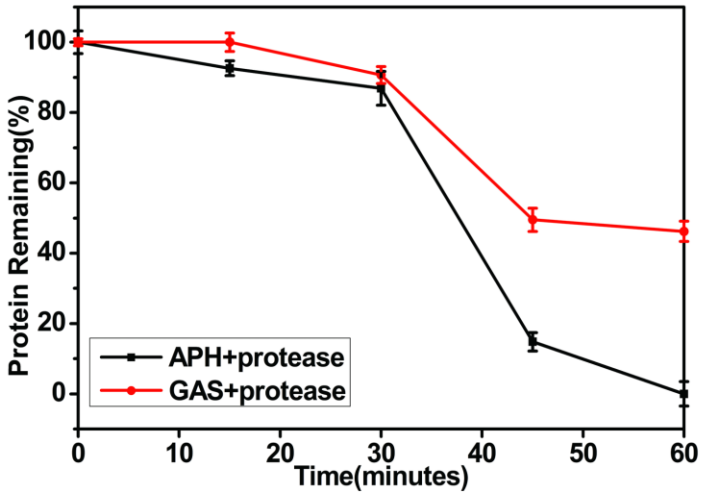

Figure S6. Stability of APH and GAS was measured the retained activity after they had been subjected to proteolytic degradation, suggesting mobilization prevents the protease from degrading the APH. Error bars indicate the standard deviation from three independent experiments.

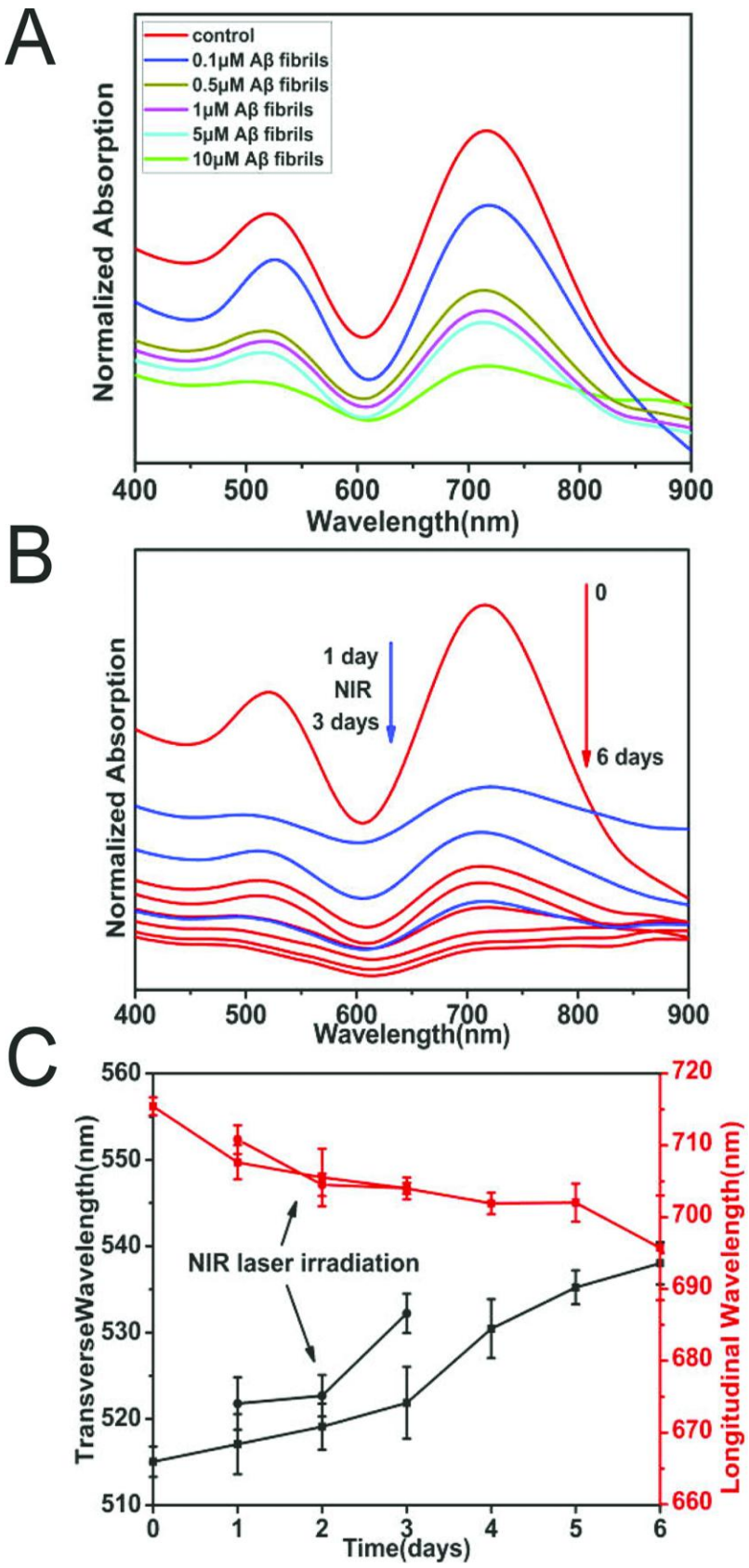
A
control
0.1μM Aβ fibrils
0.5μM Aβ fibrils
1μM Aβ fibrils
5μM Aβ fibrils
10μM Aβ fibrils
Normalized Absorption
400
500
600
700
800
900
Wavelength(nm)
B
0
1 day
NIR
3 days
6 days
Normalized Absorption
400
500
600
700
800
900
Wavelength(nm)
C
560
550
540
530
520
510
TransverseWavelength(nm)
720
710
700
690
680
670
660
Longitudinal Wavelength(nm)
NIR laser irradiation
0
1
2
3
4
5
6
Time(days)

Figure S7. Influence of Aβ1-40 aggregates on the absorption spectrum of GAS. (A) Absorption spectrum of GAS in the presence of different concentration of Aβ1-40 fibrils. (B) Recovery of absorption spectrum for the first three days' samples in the presence of GAS upon NIR laser irradiation. (C) Shift of transverse and longitudinal plasmon bands during the Aβ fibrillogenesis process in the presence of GAS and exposure to NIR laser for the first three days' samples.

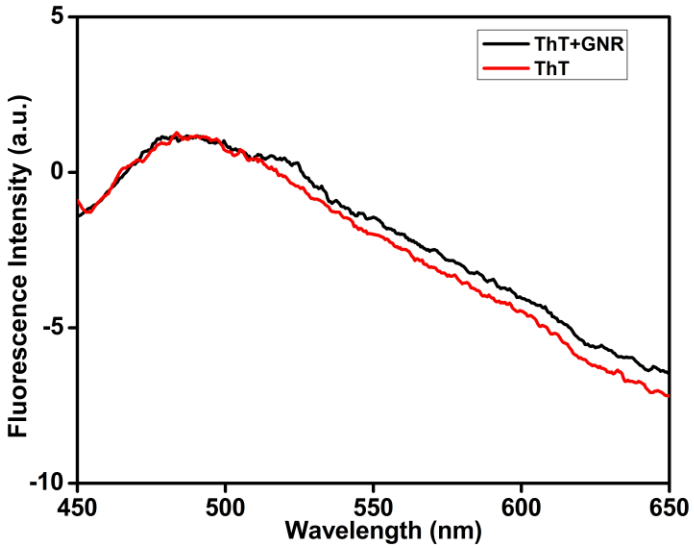

Figure S8. Fluorescence spectra of ThT in the presence or absence of GNRs.

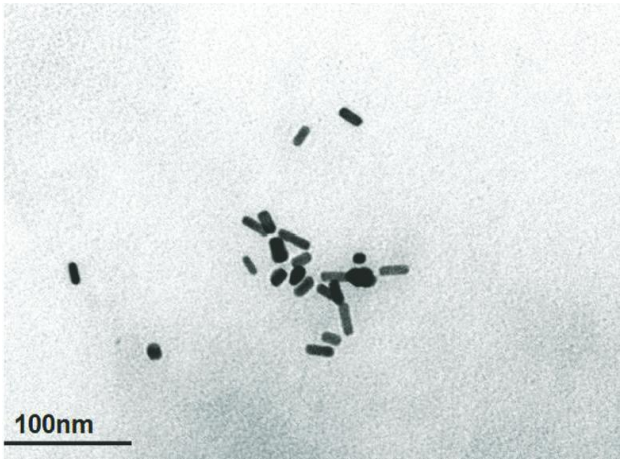

Figure S9. Inhibitory effect of GAS on Aβ monomers for another two days as monitored by TEM.

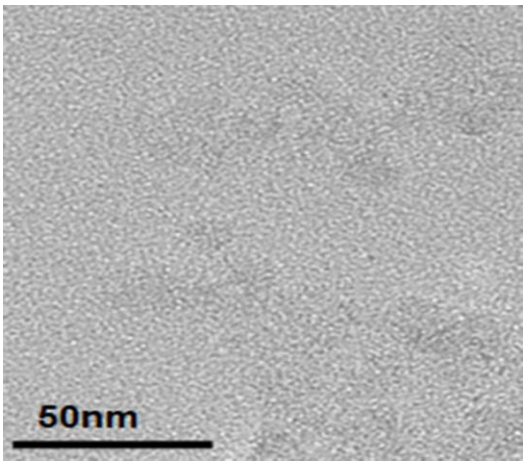

Figure S10. The sustainable inhibitory effect on Aβ fibrils formation after removal of GAS as monitored by TEM.

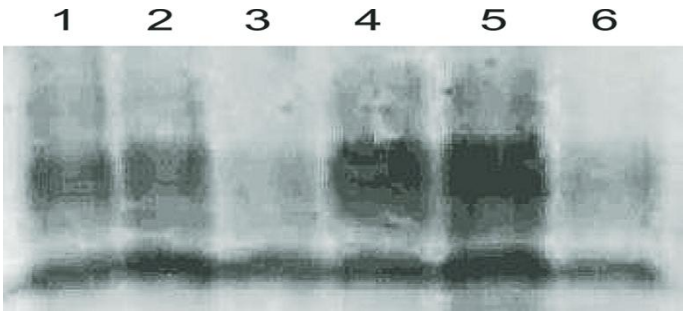

Figure S11. Western blot assay for testing anti-Aβ ability of GAS. Lane 1: Aβ oligomers incubated with 40ug/ml GAS; Lane 2: Aβ fibrils incubated with 40ug/ml GAS. Lane 3: Aβ monomers incubated with 40ug/ml GAS. Lane 4: Aβ oligomers alone; Lane 5: Aβ fibrils alone. Lane 6: Aβ monomers alone. Each sample containing GAS was exposure to NIR laser irradiation for 5 minutes per day and was observed on the seventh day.

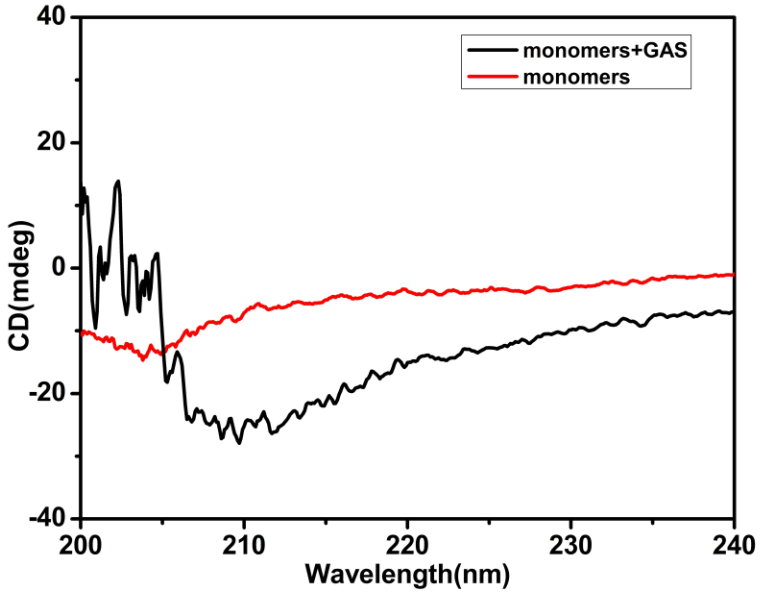

Figure S12. CD spectra of Aβ monomers in the absence or presence of GAS.

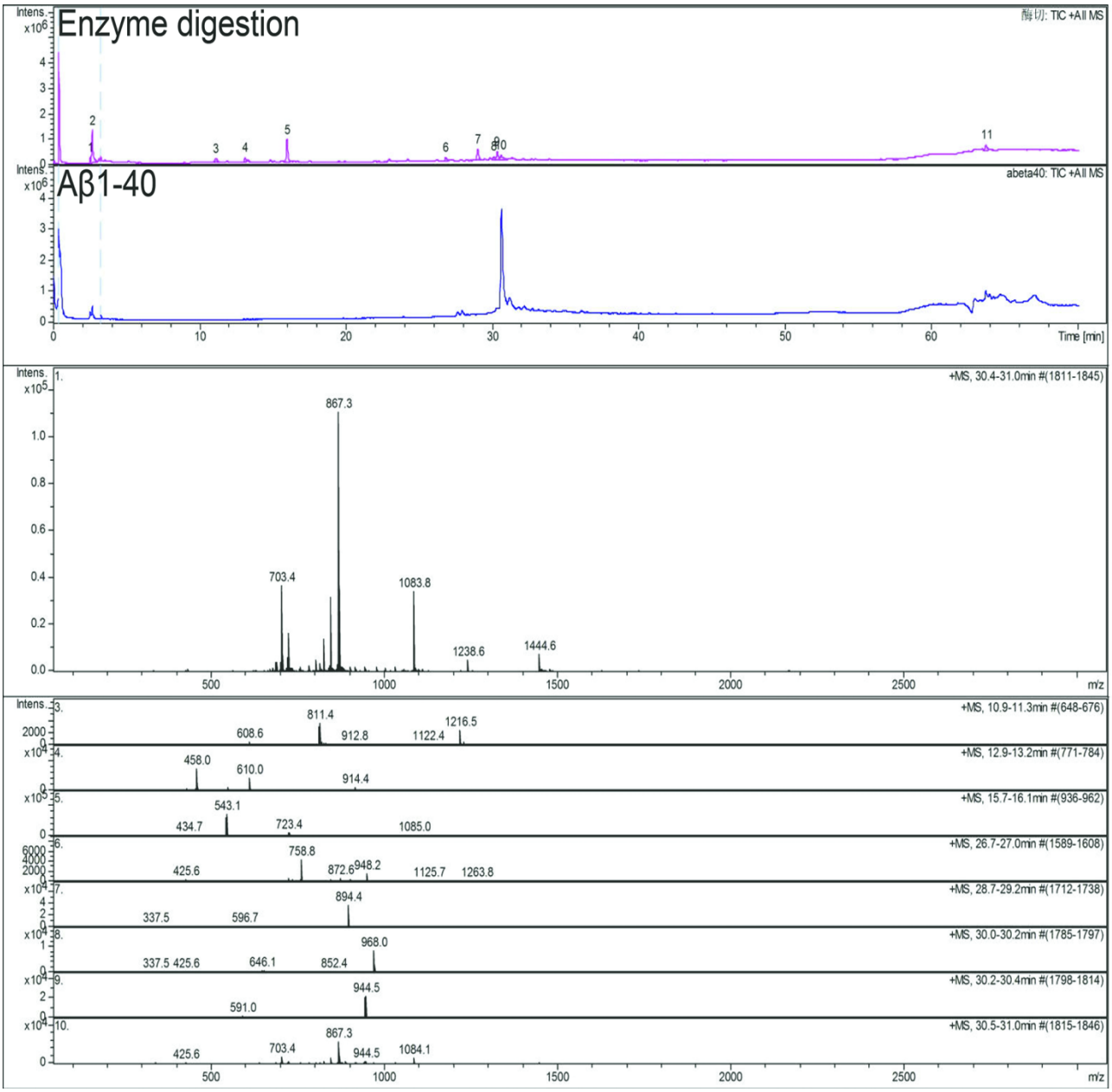

Figure S13. HPLC-MS analysis of soluble Aβ1-40 digested by APH. All three samples were incubated simultaneously for 20 hours at 37℃.

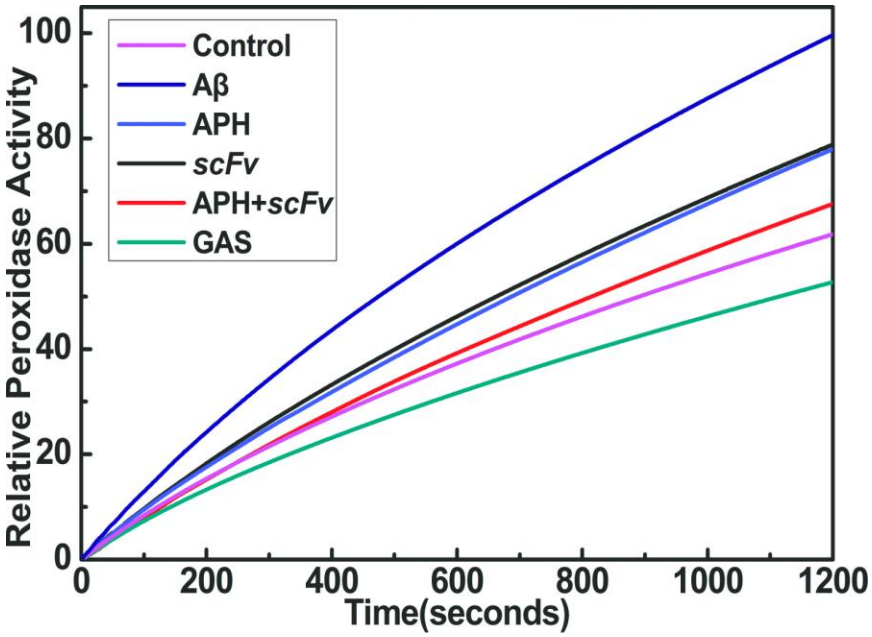

Figure S14. Effect of GAS, APH, *scFv* and the combination of APH and *scFv* on the inhibition of Aβ induced peroxidase activity, monitoring the increase of the 420nm absorption intensity.

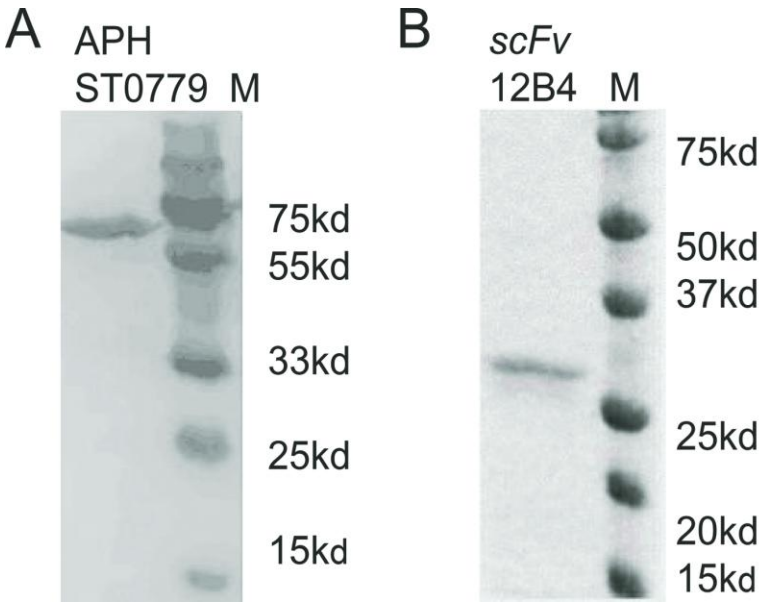

Figure S15. Protein purity of APH ST0779 and *scFv* 12B4 by Ni-NTA affinity chromatography.